J Mater Sci (2021) 56:746–761

Materials for life sciences

Antifouling nanoporous diamond membrane for enhanced detection of dopamine in human serum

Haichao Li[1], Jun Cao[1], Qiuping Wei[1,*], Li Ma[1], Kechao Zhou[1], Zhiming Yu[1], Sichao Zeng[1], Ruitong Zhu[1], Wanlin Yang[1], Cheng-Te Lin[2], and Lingcong Meng[3]

[1] *State Key Laboratory of Powder Metallurgy, School of Materials Science and Engineering, Central South University, Changsha 410083, People's Republic of China*

[2] *Ningbo Institute of Materials Technology and Engineering, Chinese Academy of Sciences, Ningbo 315201, People's Republic of China*

[3] *School of Chemistry, University of Southpton, Southampton SO17 1BJ, UK*

Received: 2 July 2020
Accepted: 15 September 2020
Published online: 1 October 2020

ABSTRACT

In vivo tracking or in vitro real sample analysis by electrochemistry is one of the most straight and useful methods in biosensor field. However, surface biofouling of electrodes by non-specific protein adsorption is inevitable and usually leads to a decrease in sensitivity. Here, we developed a Nafion-coated porous boron-doped diamond (NAF/pBDD) electrode with hydrophobic nanostructures to minimize the biofouling effect and selectively detect dopamine (DA). Larger active area was obtained by this procedure compared to a bare diamond electrode. The as-prepared electrode shows excellent antifouling property and enrichment capacity toward selective detection of dopamine (DA). The low background current of the BDD electrode and the enhanced signals enables a lower detection limit, 42 nmol L^{-1}, and a wider linear range, 0.1–110 μmol L^{-1}, for determination of DA in human serum. Additionally, the facile modified electrode demonstrated renewable property and long-term stability due to the fact that the antifouling nanostructures belong to its own.

Introduction

In vivo monitoring or in vitro sensing by electrochemical techniques is becoming a powerful tool in biological environment analysis, helping us better understand the correlation between chemistry and behavioral, diagnose signals and disease level [1–9]. However, surface biofouling of sensors still hinders their further applications due to the fouling-induced decrease in sensitivity and limited long-term functionality [10–12]. Non-specific protein adsorption on the device surface is the initial stage of many fouling mechanisms and that will ultimately compromise the

Handling Editor: Annela M. Seddon.

Address correspondence to E-mail: qiupwei@csu.edu.cn

https://doi.org/10.1007/s10853-020-05344-5

functionality of the device [4, 13]. Two major strategies have been taken to alleviate the adsorption and improve the biocompatibility of devices [10, 14]. The first approach is surface coating by electrically neutral hydrophilic polymers, which minimizes the close reactions between proteins and devices surfaces. Many of these, such as poly (ethylene glycol) (PEG) and poly(lactic-co-glycolic acid) (PLGA), have demonstrated promising results in resisting proteins adsorption [15, 16]. However, the presence of blood components or other interferents that can interact with the surface layers which have high water uptake may alter the surface that is actually applied to the biological environment; key proteins like hydrophilic ones and phospholipids can still eventually adsorb under conditions that initiate the platelet adhesion and activation [17–21]. Another method is surface patterning with hydrophobic nanostructures, which can effectively minimize the amount of proteins actually arriving at the surface by reducing the length of diffusive transport region [22–25]. Different grain sizes of silica, metal particles and carbon-based materials have been decorated on the substrate to create surfaces with different roughness. Although these structures show excellent antifouling property because they can prevent proteins from reaching electrode inner surface, they still face a great challenge in preparing methods by a controllable manner (e.g., nanoporous gold) [5, 26–30].

Typically, surface biofouling of sensors is one of the most serious issues challenging determination of dopamine (DA), which is an important monoamine neurotransmitter. Because Parkinson's, Alzheimer's and Huntington's diseases could be monitored by the abnormal DA level [3] due to its vital role in central nervous, renal and hormonal systems. But the concentration of DA in brain is low and its action depends on the overall levels and short bursts. Thus, diagnosis of these diseases necessitates very accurate measurements of DA in biological samples and the electrochemical analysis of DA could be hindered easily by serious biofouling of the electrodes [4, 13]. Besides, the close oxidization potentials of DA and AA make it difficult to distinguish DA from interferents and extra DA could be produced by the reaction of the unoxidized AA and the oxidation products of DA then reoxidized at electrode surface (EC′ mechanism) [31, 32]. As a strong candidate for biosensing material, boron doped diamond (BDD) stands out due to its low adsorption property, inherent robustness, wide potential window and good biocompatibility [27, 33–38]. Fewer surface functional groups of diamond electrode are able to reduce the adsorption of oxidation products [38, 39]. However, BDD electrodes are incompetent when it comes to antifouling to proteins due to their fierce responses and strong adhesion in biological environment [11, 40]. Therefore, further modifications or patterning is usually required. Herein, we report a nanoporous diamond surface as a new antifouling material for enhanced, selective detection of dopamine in human serum. We expect that a nanoporous diamond electrode will potentially reduce the nonspecific adsorption of proteins and bring a new inspiration for improving the performance of biosensors. Nevertheless, the use of a nanoporous diamond electrode for antifouling to proteins adsorption has not been reported.

In this work, we use facile thermal etching technique to create a hydrophilic nanoporous diamond surface. The prepared Nafion-coated porous boron-doped diamond (NAF/pBDD) electrode shows high selectivity and stability for detection of DA in human serum, being unaffected by the excess interferences of AA. Most importantly, antifouling properties and stability analysis of this electrode show the potential of real applications.

Experimental methods

Materials

Dopamine hydrochloride (≥ 99%), *L*-ascorbic acid (≥ 99%) were purchased from Sigma-Aldrich, United States. Nafion PFSA 5% dispersions D-520 (Dupont, United States) were obtained from ILongSheng energy technology Co. Ltd., Suzhou, China. Phosphate buffers (pH 7.4, 0.01 mol L^{-1}) were purchased from Leagene Biotechnology, Beijing, China. Normal human serum was purchased from Abbkine Scientific Co., Ltd, Wuhan, China. All reagents were of analytical grade and used as received without any further purification. All solutions were prepared with deionized, distilled water (18 MΩ cm resistance).

Apparatus

Morphology studies were conducted using a scanning electron microscope (SEM) (FEI Quanta FEG

250, United States and TESCAN MIRA3, Czech Republic). Raman spectroscopic analysis was carried out using LabRAM HR800, HORIBA Jobin–Yvon, France. Electrochemical measurements were finished by an electrochemistry workstation CHI660e, (Chen-Hua, Shanghai, China). The BDD, pBDD, NAF/pBDD electrodes were used as the working electrodes, and an Ag | AgCl | $KCl_{(3.5\ mol)}$ electrode and a platinum plate ($10 \times 10 \times 3\ mm^3$) were used as the reference and auxiliary electrodes, respectively.

Preparation of Electrodes

The boron doped diamond (BDD) layer was grown on p-type silicon wafer substrates ($4 \times 4\ mm^2$) using a hot filament chemical vapor deposition (HFCVD) system. Before the deposition, the substrates were ultrasonically cleaned with acetone, ethanol and deionized water for 20 min individually, and then ultrasonically treated in the suspension of diamond nanopowder and deionized water for 40 min and 2 min, respectively. During the 8-h deposition, the BDD film was deposited on silicon substrates in the mixture gases of CH_4 (1 sccm), H_2 (49 sccm) and B_2H_6 (0.3 sccm) under 3.0 kPa, maintaining the temperatures of the substrate and a tungsten filament at 850 °C and 2350 °C, respectively. The porous BDD (pBDD) was prepared by a thermal catalytic etching (TCE) process, which includes: (1) sputtering a nickel layer on the BDD layer using a physical vapor deposition (PVD) system, (2) heat treatment of the Ni/BDD in a quartz tube furnace in H_2 and (3) removing remaining Ni. The details of the TCE were given in our earlier work [37]. The Nafion 5% dispersions were diluted to 0.5 wt% using isopropanol and then drop-coated on the pBDD layer using an adjustable micro-pipettor. The renewable process of the electrodes was finished by cleaning in ethanol at 70 °C for 5 min and then ultrasonic treatment (60 Hz) in distilled water for 10 min.

Results and discussion

Characterizations of electrodes

The preparation processes of the BDD, pBDD electrodes were illustrated in Fig. 1a; the pBDD electrode was obtained by thermal etching after the deposition of BDD film. The morphology of the BDD, pBDD and NAF/pBDD electrodes was examined by SEM analysis. Figure 1b, c shows the micro-crystal diamond layer deposited on the silicon substrate. The diamond layer is well covered on the substrate, and the grains size are about from 3 to 5 μm. The porous diamond obtained by thermal etching is presented in Fig. 1e and f. The nanopores on the diamond are well dispersed on the crystal plane after removing the Ni nanoparticles using the nitric acid. These nanopores are supposed to increase the electrochemically active surface area (EASA) by producing more defect sites on the surface of the electrode. The Raman spectra for the BDD, pBDD and NAF/pBDD electrodes are presented in Fig. 1h. The strong peak at $\sim$ 466 cm^{-1} and $\sim$ 1192 cm^{-1} are the boron band, which has no obvious change in three electrodes due to their same boron-doped concentrations [41]. The relative weaker peak at $\sim$ 1063 cm^{-1} is from the Nafion membrane, corresponding to the symmetric stretch of sulfonic group [42]. The peaks at $\sim$ 1291 cm^{-1} are assigned to the diamond phase. This peak shifted significantly from 1332 to 1291 cm^{-1} due to the high B/C ratio (B/C = 20,000 ppm in this work). Generally, polycrystalline boron-doped diamond films show a Raman spectrum where the 1332 cm^{-1} diamond vibrational mode peak intensity decreases and shifts down in its wave number with the increasing boron concentration [43]. It would appears only as a shoulder when the B/C ratio exceeds 12,000 ppm [44]. The X-ray diffraction (XRD) patterns for the BDD, pBDD and NAF/pBDD electrodes are shown in Fig. 1i. Two peaks at 4° and 7° could be found at all three electrodes which can be assigned to the (111) and (220) of diamond. On the BDD and pBDD electrodes, there is a common peak at 69.5° from the silicon carbide. The etching process for the nanopores results in the graphite peak at 9.5° on the pBDD electrode. And due to the Nafion membrane covered on the NAF/pBDD electrode, the intensity of two peaks for diamond decreases and the peaks for silicon carbide and graphite could not be found. Furthermore, there is a broad peak at 17° on NAF/pBDD electrode which could be assigned to the semi-crystalline structure of the Nafion's main chain [45].

Electrochemical characterization of different electrodes

The cycle voltammetry (CV) and electrochemical impedance spectrum (EIS) were employed to

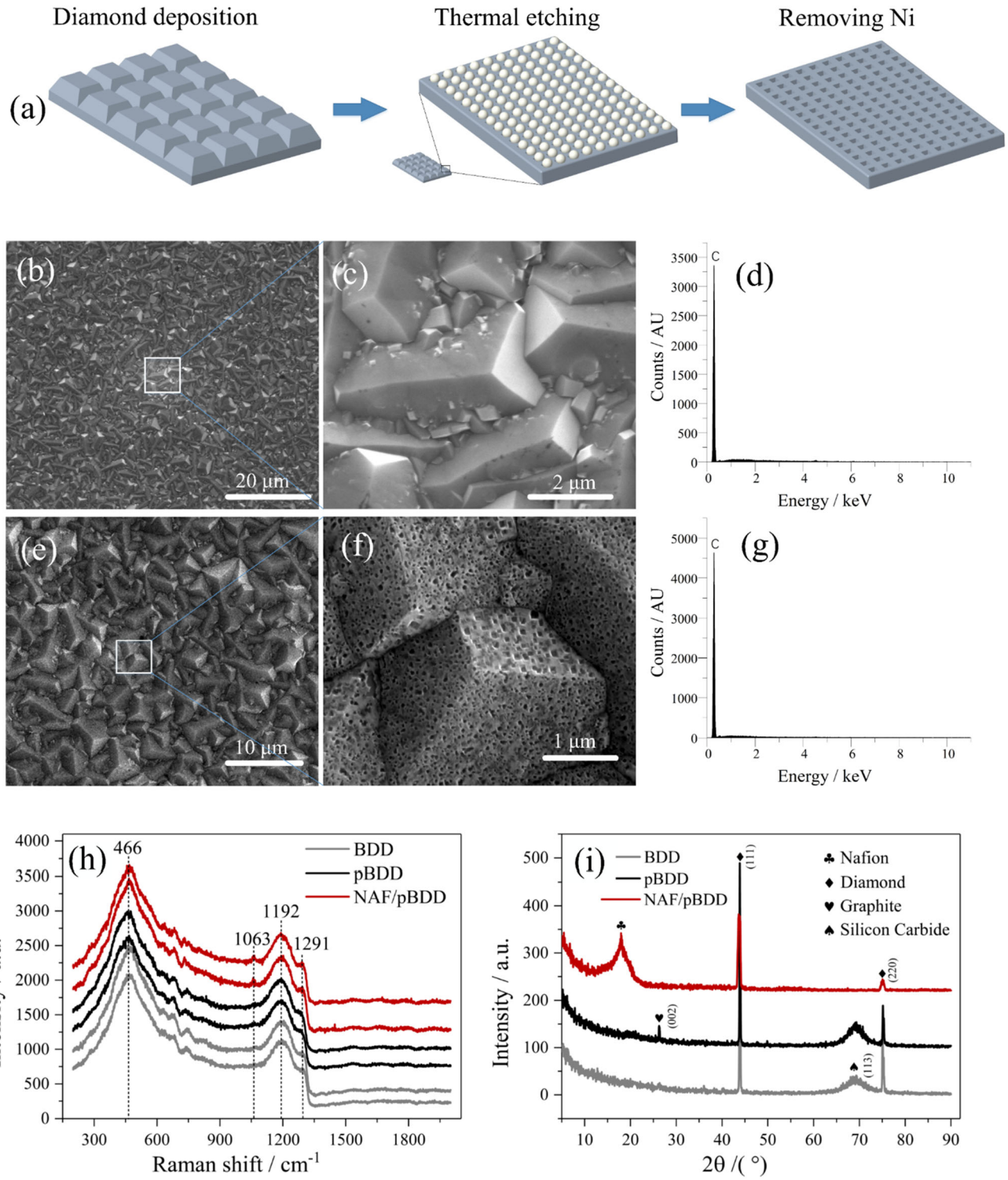

Figure 1 Schematic diagram **a** for the preparations of the BDD, Ni/BDD and pBDD electrodes; SEM images for BDD electrode (**b**, **c**), and pBDD electrode (**e**, **f**); EDS for BDD electrode (**d**) and pBDD electrode (**g**); **h** The Raman spectra for the BDD, pBDD and NAF/pBDD electrodes; **i** The X-ray diffraction (XRD) patterns for the BDD, pBDD and NAF/pBDD electrodes.

evaluate the surface nature and electron transfer behavior BDD and pBDD electrodes. Figure 2a shows comparative CV responses of BDD and pBDD electrodes in a 2 mmol L^{-1} $K_3[Fe(CN)_6]$ at a scan rate 10

mVs^{-1}. The higher peak current magnitudes and smaller ΔE_p values with pBDD electrode could be due to the facile electron transfer behavior and its larger electrochemically active surface area (EASA). The EASA was then estimated according to the Randles-Sevcik equation:

$$I_p = 2.69'10^5 n^{3/2} A D^{1/2} C v^{1/2}$$

where n is the number of electrons participated in the redox reaction, A is the EASA (in cm^2), D is the diffusion coefficient ($D = 6.50 \times 10^{-6}$ cm^2 s^{-1}) [46], C is the bulk concentration (in mol cm^{-3}), v is the scan rate (in V s^{-1}). Larger EASA value for the pBDD electrode (0.14 cm^2) than these of the BDD electrode (0.08 cm^2), reveal that the EASA was substantially increased by these nanopores obtained through etching. The EIS data for two electrodes were obtained at an open circuit potential of 10 mV in the frequency range from 1 Hz to 1 MHz, as presented in Fig. 2b through the Nyquist diagrams. The well-defined semi-circles at high frequencies for these electrodes correspond to the electron transfer process and the diameters are equivalent to the charge transfer resistance (R_{CT}). The impedance parameters were evaluated using a curve fitting software and the values were noted to be 8.8 Ω and 4.5 Ω for BDD and pBDD electrodes, respectively. The lower R_{CT} value for pBDD electrode reveals that the electron transfer resistance was reduced by these nanopores due to its excellent conductivity and a large number of defect sites.

The heterogeneous electron transfer rate constants (k^o, cm^{-1}) have been calculated by the extended method which merges the Klingler-Kochi and Nicholson and Shain methods for totally irreversible and reversible systems [47–49], using following equation:

$$\Psi = k^{\circ}[pDmnF/RT]^{-1/2}$$

where ψ is the Nicholson's kinetic parameter dependent on ΔE_p, m is the number of electrons transferred in the oxidation/reduction process (here, m = 1), R is the universal gas constant, and T is the temperature (in Kelvin). Values of ψ were determined for every scan rate in the range 0.01–0.15 Vs^{-1} from Lavagnini's equation:

$$\Psi = (-0.6288 + 0.0021X)/(1 - 0.017X)$$

where X indicated $\Delta E_p \times n$ expressed in mV [50, 51]. The value of k° was obtained to be 1.59×10^{-3} cm s^{-1} and 0.87×10^{-3} cm s^{-1} from the slope of ψ vs $[\pi DnvF/RT]^{-1/2}$ plots, for pBDD, BDD electrodes, respectively, as shown in Figure S1. The k^o value obtained in the case of the pBDD electrode resulted to be higher than that obtained in the case of the BDD electrode, showing the nanopores with new formed defect sites on the pBDD are helpful to a faster electron transfer kinetics.

Electrocatalytic oxidation of DA, AA on the BDD, pBDD and NAF/pBDD electrodes

The electrochemical behaviors toward DA and AA of BDD, pBDD and NAF/pBDD electrodes were then investigated using cyclic voltammetry (CV) and square-wave voltammetry (SWV). The individual CV responses to the two biological fluids are presented in Fig. 3b, c. On the bare BDD electrode, the oxidation potential of DA and AA are ~ 0.37 and ~ 0.74/V vs Ag | AgCl | KCl $_{(3.5\ mol)}$, but no clear separative peaks were found when applying to mixed solution

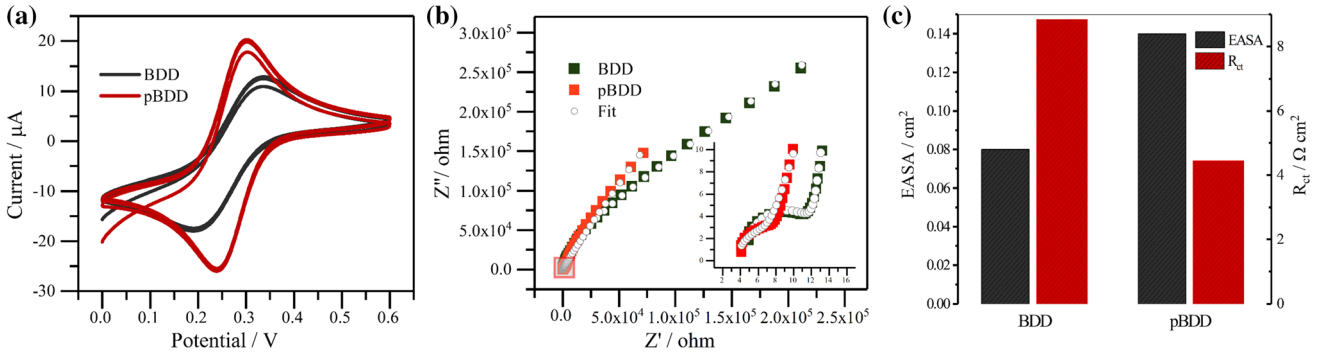

Figure 2 The CVs (**a**) and the EIS (**b**) for the BDD and pBDD electrodes with 2 mmol L^{-1} of $K_3[Fe(CN)_6]$ in 0.1 mol L^{-1} KCl solution; **c** The comparations of EASA and R_{ct} for BDD and pBDD electrodes.

(Fig. 3b). This could be assigned to the limited active sites on BDD electrode, resulting in the low catalytic capability. More negative oxidation potentials (~ 0.36, ~ 0.70/V vs Ag | AgCl | $KCl_{(3.5\ mol)}$ for DA, and AA) were reached on the pBDD electrode, but still, the overlapped potential of DA and AA exists (Fig. 3c). The lower oxidation potentials and higher response currents are attributed to the nanopore structure on the pBDD electrode, but the intrinsic property of diamond determines the non-selective behavior [52]. Besides, the EC′ mechanism mentioned in the introduction, an extra reaction between AA and the oxidation products of DA, dopamine-o-quinone, still exists. The EC′ effect, as shown in Fig. 3a, would produce new DA and the reoxidized DA will result in an interference signals to DA detection [31, 32].

Two main strategies have been adopted to address this problem. One is using nanomaterial with high catalytic activity to modify the surface of diamond electrode and oxidizing AA before DA. Recently, several studies modifying carbon black, carbon nanotubes and graphene on diamond to selective determination of DA in AA are all based on this strategy [46, 53]. But the depletion of AA near the surface of electrodes is not equivalent to the total oxidization of AA and there could still be some influence on the signal of DA. Very recently, an increase in the signals of DA was found by other researchers when in the presence of AA on a gold electrode modified with graphene, which indicated that using the depletion effect of AA to eliminate EC′ effect could be unreliable and more work is still needed to study further. Another strategy is employing the functional membrane covered on the diamond electrode such as Nafion to separate DA and AA and selectively obtain the signals of DA oxidation only (Scheme 1). Nafion membrane has unique ionic properties as a cation exchange polymer, which could be attributed to incorporating perfluorovinyl ether groups terminated with sulfonate groups onto a tetrafluoroethylene (PTFE) backbone and as such the pK_a of the sulfonic

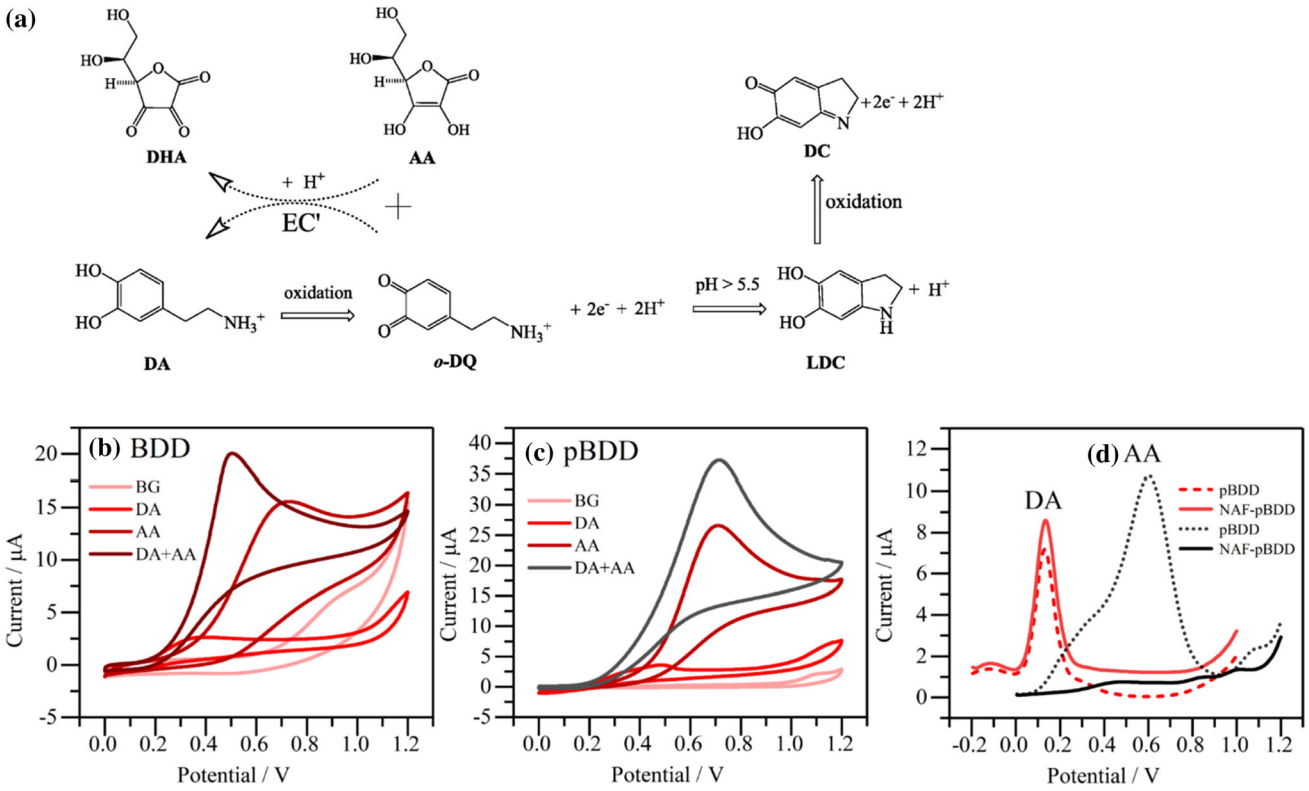

Figure 3 **a** Schematic diagram for DA oxidation pathway and the EC′ effect; CVs of individual determination of three analytes at BDD electrode (**b**) and pBDD electrode (**c**) in 0.01 mol L^{-1} PBS (pH 7.4) containing 1 mmol L^{-1} AA, 20 μmol L^{-1} DA and their mixed solution respectively at 50 mVs^{-1}. **d** SWVs of individual determination of DA and AA at pBDD electrode and Nafion coated NAF-pBDD electrode in 0.01 mol L^{-1} PBS (pH 7.4) containing 1 mmol L^{-1} AA and 20 μmol L^{-1} DA. Square-wave voltammetry (SWV) was employed the following parameters: 30 mV amplitude, 8 mV step potential, and frequency of 5 Hz.

acid moiety is estimated at − 6, enabling the functional group to deprotonate within the physiological pH range [7, 8]. At a physiological condition, DA is positively charged, but AA is negatively charged [54]. Naturally, anions like AA will be rejected by the negative charge from the Nafion at the surface of electrode, and the interference signals will be eliminated. On the other hand, positively charged DA will be attracted to enhance the analyte signal (Scheme 1). Herein, we evaluated the influence of Nafion membrane on the signals of DA and AA, which is coated on the pBDD electrode. 2 μL 0.5 wt% Nafion solution were coated on the surface of an as-prepared pBDD electrode, and this electrode was employed to detect 20 μmol L^{-1} DA and 1 mmol L^{-1} AA solution. The SWV signals are shown in Fig. 3d. The oxidation current of DA was enhanced due to the larger active area of the pBDD electrode. On the contrary, the response current of AA was suppressed from 10.5 to 0.9 μA. And the signal for the mixed solution of DA and AA are 11.3 μA, just 0.8 μA higher than the single DA, which indicates that it is practicable to eliminate the impact of AA in the mixed solution by Nafion modification when selectively detecting DA (Scheme 1).

As discussed above, DA in the mixed solution could be detected independently by employing the NAF/pBDD electrode, being nearly unaffected by the interferences from AA. But apparently proper amount of Nafion and well coverage of the Nafion membrane coated on the diamond layer are essential conditions for a selective and accurate determination of DA. The SEM images for the diamond electrode modified by certain amount of Nafion are shown in Fig. 4a–c. The Nafion membrane is even and well covered on the diamond layer (Fig. 4a). But it is difficult to obtain a neat cross plane for this three-layer electrode due to the brittleness of silicon substrate and diamond layer and the flexibility of the polymeric Nafion membrane. Thus, we created a small crack by punctured on the Nafion membrane using a micro-needle (Fig. 4b, c). The profile of the crystal grains of diamond can be seen in Fig. 4c, which can indirectly prove the good uniformity of the Nafion membrane. And the thickness of Nafion layer could be estimated at around a few microns to tens of microns. Obviously, the precise control of the thickness of Nafion layer will determine a more stable performance of the NAF/p-BDD electrode. Thus, adding volumes of Nafion are crucial and must be optimized. 0–10 μL Nafion solution were added to and dried on 7 same p-BDD electrodes and the SWV signals to individual DA (20 μmol L^{-1}) and AA (1 mmol L^{-1}) were investigated. For DA, peak

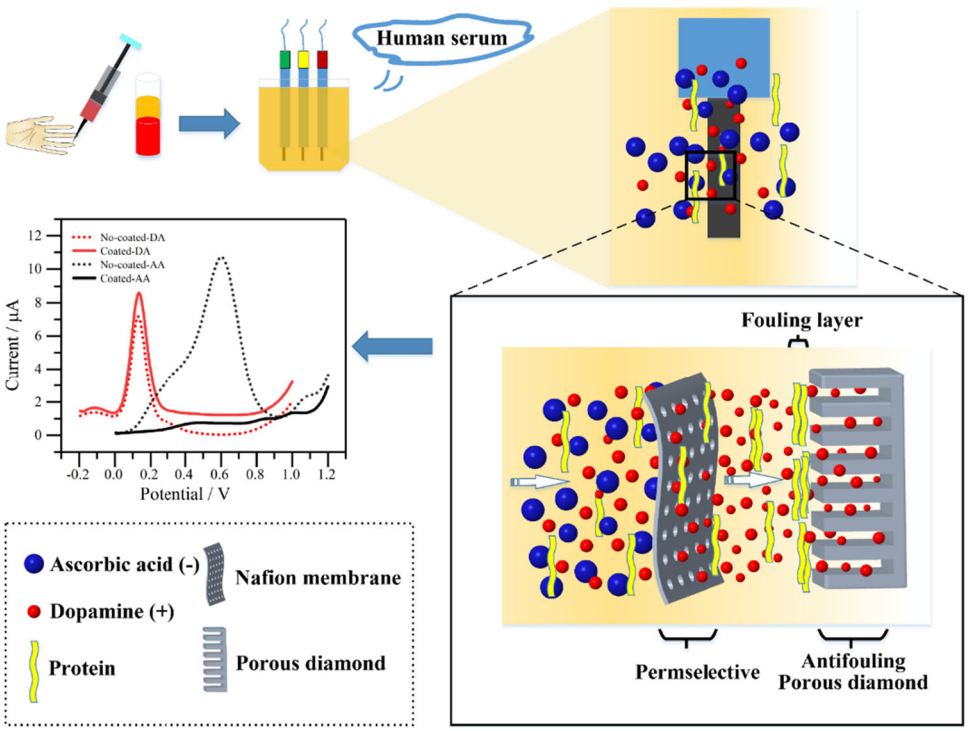

Scheme 1 Illustration of mechanism of the antifouling property and the selective detection of DA on the NAF/pBDD electrode.

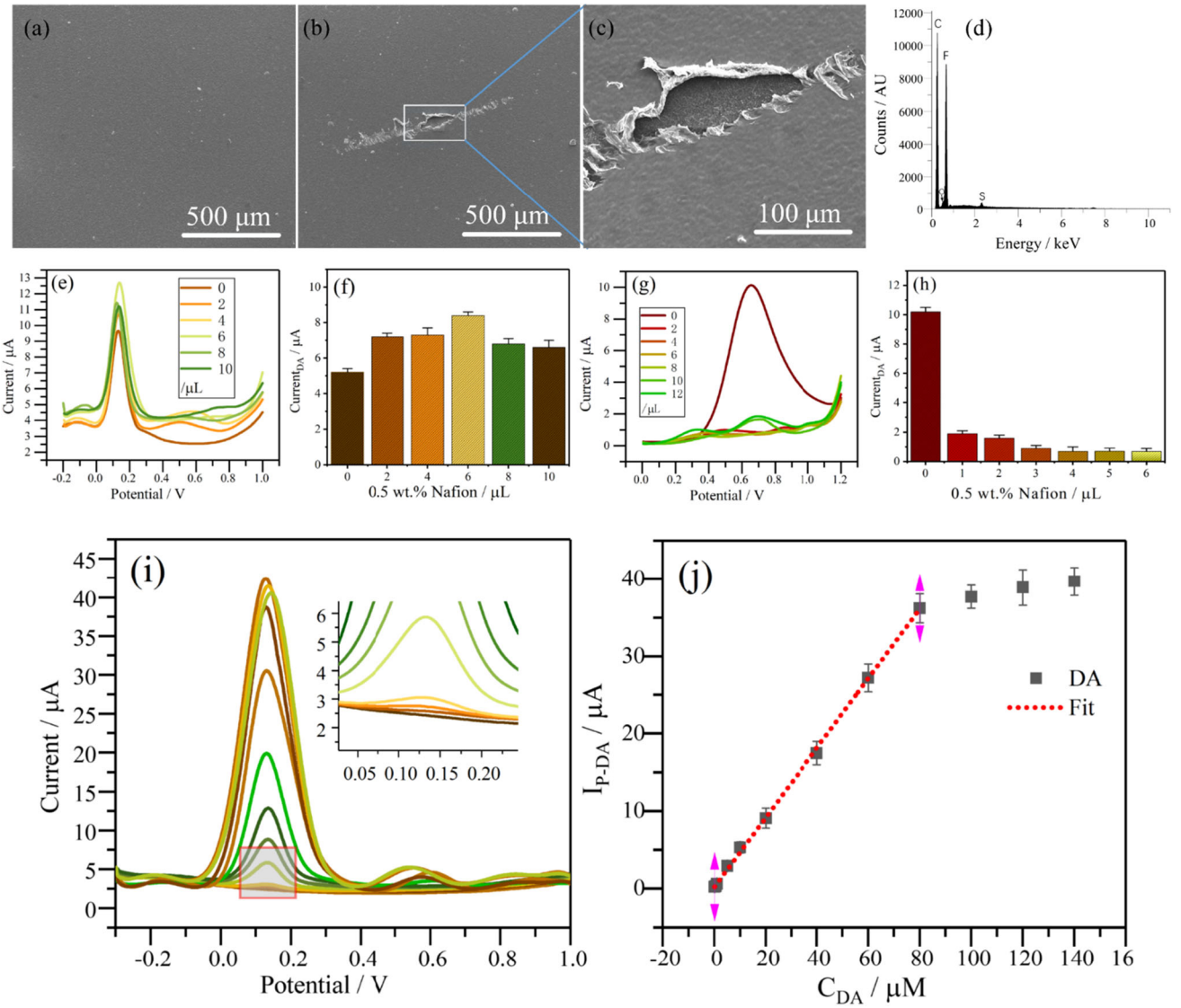

Figure 4 **a** SEM image for the NAF-pBDD electrode; **b** SEM image for the NAF-pBDD electrode with a small crack punctured using a microneedle; **c** The enlarged view of the small crack; **d** The EDS for the NAF-pBDD electrode; **e** SWVs for NAF-pBDD electrodes coated with 0–10 μL Nafion solution respectively in 0.01 mol L^{-1} PBS (pH 7.4) containing 20 μmol L^{-1} DA; **f** Values of current response toward 20 μmol L^{-1} DA for NAF-pBDD electrodes coated with 0–10 μL Nafion solution respectively; **g** SWVs for NAF-pBDD electrodes coated with 0–6 μL Nafion solution respectively in 0.01 mol L^{-1} PBS (pH 7.4) containing 1 mmol L^{-1} AA; **h** Values of current response toward 1 mmol L^{-1} AA for NAF-pBDD electrodes coated with 0–6 μL Nafion solution respectively; **i** SWVs for DA in the concentration range from 0.1 to 100 μmol L^{-1} in 0.01 mol L^{-1} phosphate buffer solution containing 1000 μmol L^{-1} AA and 5 vol% human serum; **j** Peak current of DA oxidation at corresponding various concentrations of DA.

current increases with the Nafion volume added. The maximum value can be found at 6 μL, which reveals that suitable amount of Nafion could enhance the response currents for DA due to the interaction between them. But too much Nafion could weaken the response due to hindering the mass transfer due to Nafion's insulation (Fig. 4e, f). On the other hand, obvious suppression to AA could happen even with a relatively less amount of Nafion (2 μL, red curve, Fig. 4g, h) and it maintained similar effect when the addition exceeded 4 μL (Fig. 4h). Therefore, the addition of 6 μL Nafion is considered optimal for DA determination in this work.

Table 1 Detection limit and linear range at various electrodes

Sensors	Slope and sensitivity (μA (μmol cm^2)$^{-1}$)	Detection limit (μmol L^{-1})	Linear range (μmol L^{-1})	References
CB-Nafion/p-BDD	0.45, 3.21	0.042	0.1–110	This work
GE/Pt	0.34, 1.79	0.03	0.03–8.1	[57]
SPGNE	0.08, 1.14	0.12	0.5–2000	[58]
PANi/rGO	0.14, 2.01	0.5	2–18	[59]
Au@Pd-rGO	0.42, 6.08	0.024	0.1–100	[60]
RGO-ZnO	0.33, 4.68	1.08	3–330	[61]
GO-PAN	0.26, 3.71	0.5	1–14	[62]
NG	0.11, 1.57	0.25	0.5–170	[63]
MWCNT-FeNAZ–CH	0.37, 5.28	1.05	7.35–833	[64]
HCNTs	0.69, 9.85	0.8	2.5–105	[65]
PSFM	0.08, 1.14	0.3	0.05–470	[66]
AuNPs–βCD–GR	0.45, 6.43	0.15	0.5–150	[67]
NiHCF/PDAN	0.55, 7.85	0.03	600–1000	[68]
AuNPs/P(PDA)–GO	0.53, 7.57	0.02	0.05–100	[69]
Nafion/AuNPs/AzA/Ts	0.72, 10.28	0.01	0.5–50	[70]
CB/GC	0.11, 1.57	0.052	0.59–11.8	[71]

Determination of DA in the presence of AA using the NAF/pBDD electrode

In this part, the optimized NAF/pBDD electrode was employed to determine DA in a mixed solution containing AA and 5 vol% human serum. The effects of amount of Nafion on the NAF/pBDD electrode were investigated, and the optimization process are discussed in the supporting information. The addition of 6 μL Nafion is considered optimal for DA determination in this work. Figure 4i shows the SWV response for the oxidation of DA in the concentration range from 0.1 to 150 μmol L^{-1} in 0.01 M phosphate buffer solution containing 1000 μmol L^{-1} AA and 5 vol% human serum. The peak currents demonstrate a linear variation with the concentrations of DA in the range of 0.1–10 μmol L^{-1} and the correlation coefficient (R^2) is 0.998. The slope of the calibration curve is calculated to be 0.449, and the sensitivity is estimated to be 3.21 μA (μmol cm^2)$^{-1}$. The relative standard deviation (RSD, %) is 3.1%. The limit of detection (LOD) has been estimated using the following formula [55].

$$\mathrm{LOD} = 3S_b/\mathrm{m} \tag{3.1}$$

where S_b is the standard deviation obtained from 12 measurements of the background signals and m is the sensitivity represented by the slope of the calibration. The LOD is estimated to be 0.042 μmol L^{-1}.

As presented in Table 1, the slope and sensitivity, the limit of detection (LOD) and linear range of the NAF/pBDD electrode were compared with other DA sensors. The lower LOD and wide linear range could be attributed to the low background current of diamond electrode, large amounts of defect sites of nanopores and the enhancement from the Nafion layer due to the special interaction between the Nafion and DA. Although the performance of the some other sensors was better than the NAF/pBDD electrode in this work, the biocompatibility, simple structure and high stability of this electrode enable it to stand out among these. Crucially, its LOD could fits the concentrations of DA for the real-life applications, such as in human brain (0.02–0.2 μmol L^{-1}) [13] and human plasma (0.23 μmol L^{-1}) [56].

Reproducibility of the NAF/pBDD electrode in real sample and excess interferents

The real-life applicability and the feasibility in excess interferents of the NAF/pBDD electrode were exemplified by applying to detect DA in human serum and a mixture containing serum and excess AA. 1–80 μmol L^{-1} DA was added into a 5 vol% serum solution (prepared with phosphate buffers solution). All samples were diluted by 0.01 mol L^{-1} phosphate buffers solution (pH 7.4) and the SWV results are showed in Figure S2 and Table 2. The

Table 2 Recovery of Dopamine (DA) at the NAF/pBDD electrode in real samples and excess AA

Sample	Added (μmol L^{-1})	Founded (μmol L^{-1})	Recovery[a] (%)
[DA in human serum]	1	0.91	90.9
	5	5.41	108.2
	10	11.64	116.4
	20	20.33	101.6
	40	38.15	95.4
	80	80.91	101.1
[DA in human serum] + interferents[b]	1	0.97	97.5
	5	5.85	117.1
	10	11.64	116.4
	20	20.55	102.8
	40	39.48	98.7
	80	79.57	99.5

[a]Recovery % = ([analyte]Founded/[analyte]Added) × 100%

[b]Interferents containing AA (1000 μmol L^{-1}) with fixed concentrations

calculated values reveal that the fabricated NAF/pBDD electrode exhibits good reproducibility and anti-interference ability, indicating the potential application of the electrode in real samples.

Antifouling properties and stability analysis of the NAF-pBDD electrode

As mentioned in the introduction part, the first method to reduce proteins adsorption by a hydrophilic polymer could be invalid when it comes to some blood components or interference that have high water uptake. This failure can be attributed to the fact that the hydration layer formed by a hydrophilic polymer, acting as a physical and energetic barrier that minimize protein adsorption, could be destroyed by the substance with high water uptake. The protein arriving at the surface must pass three regions: the conductive transport region in blood or tissue fluid, the diffusive transport region by the assumed no-slip boundary condition and the close proximity region dominated by short range forces [10, 14, 72]. The conductive transport region is too far away for any interacting forces to contribute to the protein adsorption. But proteins will diffuse through the diffusion-controlled region, whose extent is inversely proportional to the slip length. The theory behind this method is to reduce the diffusive transport layer, caused by the no-slip condition in fluid dynamics, between the fluid and the boundary of device surface. And this approach is primarily achieved by patterning the device surface with hydrophobic nanostructures through various techniques. These hydrophobic nanostructures will create gas-fractions or air bubbles on the device surface and stabilize the surface in a dewetted state, increasing the slip length and reducing the extent of diffusive transport region. That means more proteins will be carried away from the surface by fluid as oppose to arriving at the surface through diffusion [11, 18, 20, 23]. Therefore, a hydrophobic nanoporous surface is more reliable compared to a hydrophilic polymer due to its intrinsic high stability and similar effect in most situations. The NAF-pBDD electrode in this work was designed to alleviate the protein adsorption by the nanopores and the hydrophobic hydrogen terminations on the diamond surface. Most importantly, both the nanopores and the hydrogen terminations are obtained in a simple metal thermal etching process in hydrogen environment.

To investigate the hydrophobicity of the NAF-pBDD electrode, we measured the contact angle of the BDD, pBDD, NAF-BDD and NAF-pBDD electrodes (Fig. 5). The static water contact angle of BDD electrode is much smaller than that of the pBDD electrode (52.6° vs 91.1°, Fig. 5a). This can be explained by two factors: one is the smaller roughness of the BDD electrode than that of the pBDD electrode due to the nanopores, which can reduce the extent of diffusive transport region and form a "Lotus effect" for self-cleaning; another reason is that more hydrogen terminations could be formed on the pBDD electrode after thermal etching process compared to the BDD electrode [6, 27]. The hydrogen termination on a diamond electrode has been demonstrated to be helpful in forming a hydrophobic surface [73, 74].

The hydrophobicity of a bare BDD electrode is improved by Nafion coating from 52.6° to 82.8° (comparing the BDD and NAF-BDD electrode), which is close to other researchers' results. The largest contact angle obtained on the NAF-pBDD electrode, 118.6°, and this could be attributed to the synergistic effect of Nafion membrane and the nanoporous diamond surface. Same phenomenon can be found at different time for all electrodes discussed above as shown in Fig. 5a, b.

To investigate the antifouling property of the NAF-pBDD electrode, 5 vol% human serum, used as the fouling agent, was added into DA in phosphate buffers solution (pH 7.4) (Fig. 5b). The oxidation current of DA recorded at the glass carbon electrode and graphite electrode decreased dramatically about 58% and 69% upon the addition of human serum, indicating that the serious adsorption of the proteins in human serum on these two electrodes. For a bare BDD electrode, the human serum still resulted in around 55% decrease, revealing that a bare BDD electrode is not qualified for antifouling in DA detection. In contrast, the current response on the hydrophobic pBDD and NAF-pBDD electrodes decreased only about 25% and 11%. Furthermore, the current of DA oxidation recorded on the NAF-pBDD electrode is more stable than these on the glass carbon and graphite electrodes (Fig. 5c), indicating that the products of DA oxidation do not adsorb on the NAF-pBDD electrode.

The long-term stability of the NAF/pBDD electrode was then investigated by consecutive and long-time measurements. After 50 consecutive measurements without rinsing in 30 μmol L^{-1} solution, the peak currents of DA oxidation changed slightly with a decrease in 1.3% of the initial value from 13.6 to 13.4 μA, revealing that the adsorption of the DA oxidation products is weak (Fig. 6a). The result indicates the excellent cyclic stability and good resistance to bio-fouling of the developed NAF/

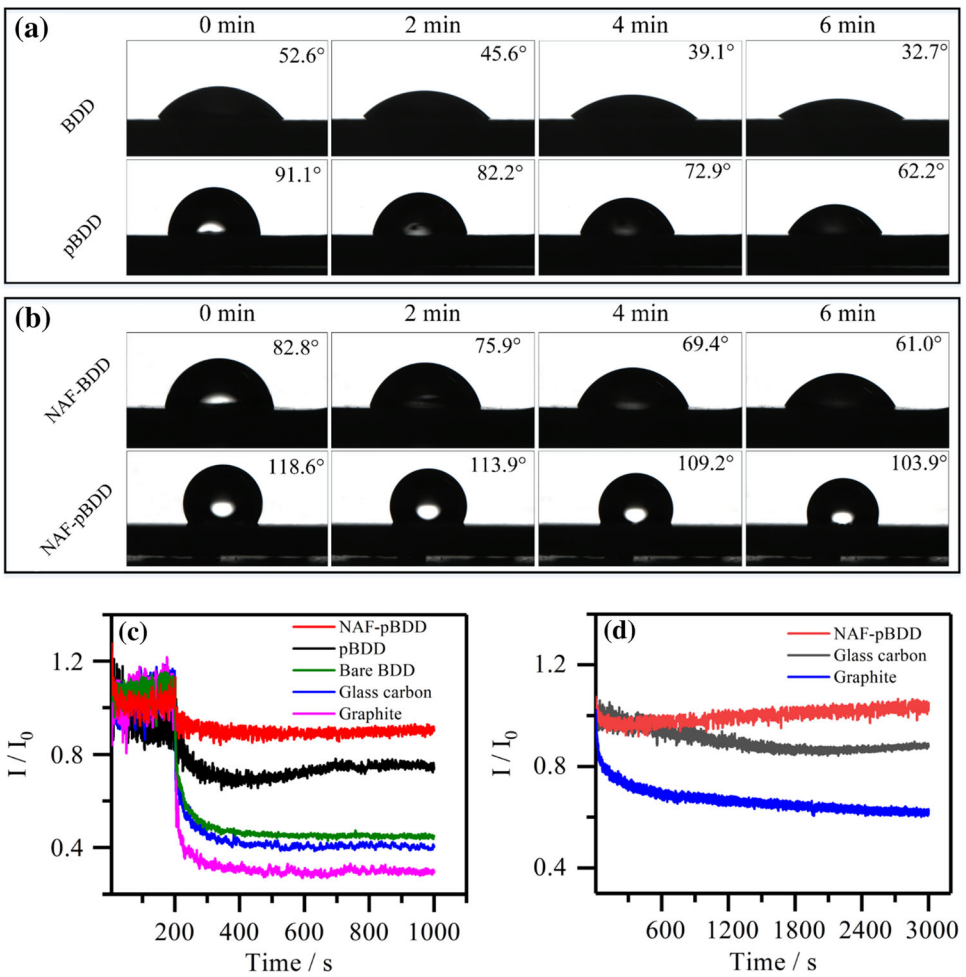

Figure 5 **a** Typical static water contact angle of the BDD, pBDD, NAF-BDD and NAF-pBDD electrodes; **b** Amperometric current response in 20 μmol L^{-1} DA solution recorded with the BDD, pBDD, NAF-pBDD, glass carbon and graphite electrodes at potential of 0.2 V upon the addition of 5 vol% human serum. **c** Amperometric current response in 20 μmol L^{-1} DA solution recorded with the NAF-pBDD, glass carbon and graphite electrodes at potential of 0.2 V. I_0 and I were the current values at starting time and given time.

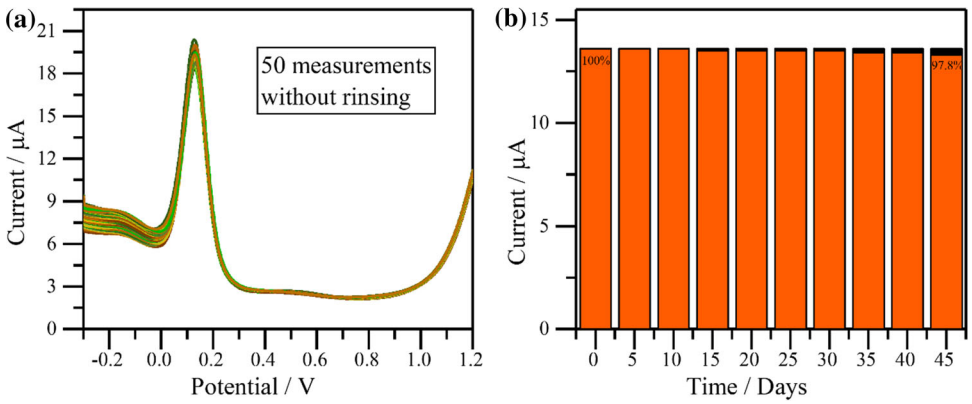

Figure 6 **a** SWVs using the NAF/pBDD electrode for 50 cyclic measurements in 50 μmol L^{-1} DA solution; **b** Peak currents of measurements in 50 μmol L^{-1} DA solution once in every day for 10 day.

pBDD electrode. The long-term stability of the NAF/pBDD electrode was studied by measurements once in every 5 days for the duration of 10 days (Fig. 6b). The peak current of the tenth day maintained approximately 94% of the initial value, demonstrating the long-term stability of this electrode. The renewable properties of the electrodes were investigated by cleaning in ethanol at 70 °C for 5 min and then ultrasonic treatment (60 Hz) in distilled water for 10 min. Five repeated experiments on a same electrode were conducted and this pBDD electrode could maintain nearly same basic electrochemical behavior, which indicated that the electrode can be reused for many times.

Conclusions

In summary, a novel porous boron doped diamond electrode modified by the biocompatible Nafion membrane was first developed to selectively detect DA in human serum and excess AA. The response current of DA was enhanced significantly by the higher surface area of the pBDD electrode due to its nanoporous structure. The elimination of the EC′ effect (interference from AA) was realized by the Nafion's suppression to AA due to its special ionic properties. High sensitivity, low limit of detection and sufficient linear range for detecting DA independently have been achieved at the optimized NAF/pBDD electrode. And this special electrode is facilely prepared, carbon based and biocompatible with a relatively low cost. Additionally, reproducibility of this NAF/pBDD electrode in human serum and excess main interferents (ascorbic acid) was validated, showing good reproducibility and anti-interference ability. The biocompatibility, antifouling property and long-term functionality of the NAF/pBDD electrode show potential for a real application and could bring a new inspiration for biosensors design.

Acknowledgement

We gratefully acknowledge the National Key Research and Development Program of China (No. 2016YFB0301400), the National Natural Science Foundation of China (Nos. 51601226, 51874370), the Natural Science Foundation of Hunan Province (Nos. 2019JJ40375, 2019JJ50793) and the State Key Laboratory of Powder Metallurgy for financial support. The authors also wish to thank the reviewers and editor for kindly giving revising suggestions.

Author contributions

HL is the first author of this manuscript. HL and QW wrote the paper and revised the manuscript at all stages. JC, LM and SZ helped the mechanism explanation and assisted with the experiments. WY and RZ provided some constructive suggestions. ZY and KZ supervised this study.

Compliance with ethical standards

Conflict of interest The authors declare no competing financial interest.

Electronic supplementary material: The online version of this article (https://doi.org/10.1007/s10853-020-05344-5) contains supplementary material, which is available to authorized users.

References

[1] Frost M, Meyerhoff ME (2006) In vivo chemical sensors: tackling biocompatibility. Anal Chem 78:7370. https://doi.org/10.1021/ac069475k

[2] Rong G, Corrie SR, Clark HA (2017) In vivo biosensing: progress and perspectives. ACS Sensors 2:327. https://doi.org/10.1021/acssensors.6b00834

[3] Nutt JG, Wooten GF (2005) Diagnosis and initial management of Parkinson's disease. N Engl J Med 353:1021. https://doi.org/10.1056/NEJMcp043908

[4] Badgaiyan RD (2013) Detection of dopamine neurotransmission in "real time". Front Neurosci. https://doi.org/10.3389/fnins.2013.00125

[5] Weng J, Xue J, Wang J et al (2005) Gold-cluster sensors formed electrochemically at boron-doped-diamond electrodes: detection of dopamine in the presence of ascorbic acid and thiols. Adv Funct Mater 15:639. https://doi.org/10.1002/adfm.200400049

[6] Tryk DA, Tachibana H, Inoue H, Fujishima A (2007) Boron-doped diamond electrodes: the role of surface termination in the oxidation of dopamine and ascorbic acid. Diam Relat Mater 16:881. https://doi.org/10.1016/j.diamond.2007.02.002

[7] Vreeland RF, Atcherley CW, Russell WS et al (2015) Biocompatible PEDOT: nafion composite electrode coatings for selective detection of neurotransmitters in vivo. Anal Chem 87:2600. https://doi.org/10.1021/ac502165f

[8] Wang HS, Li TH, Jia WL, Xu HY (2006) Highly selective and sensitive determination of dopamine using a Nafion/carbon nanotubes coated poly(3-methylthiophene) modified electrode. Biosens Bioelectron 22:664. https://doi.org/10.1016/j.bios.2006.02.007

[9] Tu NTT, Sy PC, Thien TV et al (2019) Microwave-assisted synthesis and simultaneous electrochemical determination of dopamine and paracetamol using ZIF-67-modified electrode. J Mater Sci 54:11654. https://doi.org/10.1007/s10853-019-03709-z

[10] Lin P, Lin CW, Mansour R, Gu F (2013) Improving biocompatibility by surface modification techniques on implantable bioelectronics. Biosens Bioelectron 47:451. https://doi.org/10.1016/j.bios.2013.01.071

[11] Banerjee I, Pangule RC, Kane RS (2011) Antifouling coatings: recent developments in the design of surfaces that prevent fouling by proteins, bacteria, and marine organisms. Adv Mater 23:690. https://doi.org/10.1002/adma.201001215

[12] Liu Y, Wang C, Cai N, Long S, Yu F (2014) Negatively charged gold nanoparticles as an intrinsic peroxidase mimic and their applications in the oxidation of dopamine. J Mater Sci 49:7143. https://doi.org/10.1007/s10853-014-8422-x

[13] Wightman RM, May LJ, Michael AC (1988) Detection of dopamine dynamics in the brain. Anal Chem 60:769A. https://doi.org/10.1021/ac00164a001

[14] Bhushan B, Jung YC (2011) Natural and biomimetic artificial surfaces for superhydrophobicity, self-cleaning, low adhesion, and drag reduction. Progress Mater Sci 56:1. https://doi.org/10.1016/j.pmatsci.2010.04.003

[15] Choudhary M, Brink R, Nandi D, Siwal S, Mallick K (2016) Gold nanoparticle within the polymer chain, a multi-functional composite material, for the electrochemical detection of dopamine and the hydrogen atom-mediated reduction of Rhodamine-B, a mechanistic approach. J Mater Sci 52:770. https://doi.org/10.1007/s10853-016-0372-z

[16] Mohanan VMA, Kunnummal AK, Biju VMN (2018) Selective electrochemical detection of dopamine based on molecularly imprinted poly(5-amino 8-hydroxy quinoline) immobilized reduced graphene oxide. J Mater Sci 53:10627. https://doi.org/10.1007/s10853-018-2355-8

[17] Yang C, Trikantzopoulos E, Nguyen MD et al (2016) Laser treated carbon nanotube yarn microelectrodes for rapid and sensitive detection of dopamine in vivo. ACS Sens 1:508. https://doi.org/10.1021/acssensors.6b00021

[18] Zhang M, Liao BQ, Zhou X et al (2015) Effects of hydrophilicity/hydrophobicity of membrane on membrane fouling in a submerged membrane bioreactor. Bioresour Technol 175:59. https://doi.org/10.1016/j.biortech.2014.10.058

[19] Mao LQ, Jin JY, Song LN, Yamamoto K, Jin LT (1999) Electrochemical microsensor for in vivo measurements of oxygen based on Nafion and methylviologen modified carbon fiber microelectrode. Electroanalysis 11:499. https://doi.org/10.1002/(SICI)1521-4109(199906)11:7%3c499:AID-ELAN499%3e3.0.CO;2-8

[20] Feng T, Ji W, Tang Q et al (2019) Low-fouling nanoporous conductive polymer-coated microelectrode for in vivo monitoring of dopamine in the rat brain. Anal Chem 91:10786. https://doi.org/10.1021/acs.analchem.9b02386

[21] Frost MC, Meyerhoff ME (2015) Real-time monitoring of critical care analytes in the bloodstream with chemical sensors: progress and challenges. Annu Rev Anal Chem (Palo Alto Calif.) 8:171. https://doi.org/10.1146/annurev-anchem-071114-040443

[22] Demuru S, Nela L, Marchack N et al (2018) Scalable nanostructured carbon electrode arrays for enhanced dopamine detection. ACS Sens 3:799. https://doi.org/10.1021/acssensors.8b00043

[23] Koc Y, de Mello AJ, McHale G, Newton MI, Roach P, Shirtcliffe NJ (2008) Nano-scale superhydrophobicity: suppression of protein adsorption and promotion of flow-

induced detachment. Lab Chip 8:582. https://doi.org/10.1039/b716509a

[24] Lee C, Choi C-H, Kim C-JC (2008) Structured surfaces for a giant liquid slip. Phys Rev Lett. https://doi.org/10.1103/PhysRevLett.101.064501

[25] Zhou L, Hou H, Wei H et al (2019) In vivo monitoring of oxygen in rat brain by carbon fiber microelectrode modified with antifouling nanoporous membrane. Anal Chem 91:3645. https://doi.org/10.1021/acs.analchem.8b05658

[26] Jiang T, Qi L, Qin W (2019) Improving the environmental compatibility of marine sensors by surface functionalization with graphene oxide. Anal Chem 91:13268. https://doi.org/10.1021/acs.analchem.9b03974

[27] Svitkova J, Ignat T, Svorc L, Labuda J, Barek J (2016) Chemical modification of boron-doped diamond electrodes for applications to biosensors and biosensing. Crit Rev Anal Chem 46:248. https://doi.org/10.1080/10408347.2015.1082125

[28] Wei M, Sun L-G, Xie Z-Y et al (2008) Selective determination of dopamine on a boron-doped diamond electrode modified with gold nanoparticle/polyelectrolyte-coated polystyrene colloids. Adv Funct Mater 18:1414. https://doi.org/10.1002/adfm.200701099

[29] da Silva RP, Lima AWO, Serrano SHP (2008) Simultaneous voltammetric detection of ascorbic acid, dopamine and uric acid using a pyrolytic graphite electrode modified into dopamine solution. Anal Chim Acta 612:89. https://doi.org/10.1016/j.aca.2008.02.017

[30] Lian Q, He Z, He Q et al (2014) Simultaneous determination of ascorbic acid, dopamine and uric acid based on tryptophan functionalized graphene. Anal Chim Acta 823:32. https://doi.org/10.1016/j.aca.2014.03.032

[31] Kondo T, Niwano Y, Tamura A et al (2009) Enhanced electrochemical response in oxidative differential pulse voltammetry of dopamine in the presence of ascorbic acid at carboxyl-terminated boron-doped diamond electrodes. Electrochim Acta 54:2312. https://doi.org/10.1016/j.electacta.2008.10.073

[32] Yi S-Y, Chang H-Y, H-h Cho YC, Park SH Lee, Bae Z-U (2007) Resolution of dopamine and ascorbic acid using nickel(II) complex polymer-modified electrodes. J Electroanal Chem 602:217. https://doi.org/10.1016/j.jelechem.2007.01.001

[33] Yang N, Foord JS, Jiang X (2016) Diamond electrochemistry at the nanoscale: a review. Carbon 99:90. https://doi.org/10.1016/j.carbon.2015.11.061

[34] Yuan Q, Liu Y, Ye C et al (2018) Highly stable and regenerative graphene-diamond hybrid electrochemical biosensor for fouling target dopamine detection. Biosens Bioelectron 111:117. https://doi.org/10.1016/j.bios.2018.04.006

[35] Williams OA, Nesladek M, Daenen M et al (2008) Growth, electronic properties and applications of nanodiamond. Diam Relat Mater 17:1080. https://doi.org/10.1016/j.diamond.2008.01.103

[36] Krueger A, Lang D (2012) Functionality is key: recent progress in the surface modification of nanodiamond. Adv Func Mater 22:890. https://doi.org/10.1002/adfm.201102670

[37] Mei X, Wei Q, Long H et al (2018) Long-term stability of Au nanoparticle-anchored porous boron-doped diamond hybrid electrode for enhanced dopamine detection. Electrochim Acta 271:84. https://doi.org/10.1016/j.electacta.2018.03.133

[38] Puthongkham P, Venton BJ (2019) Nanodiamond coating improves the sensitivity and antifouling properties of carbon fiber microelectrodes. ACS Sens 4:2403. https://doi.org/10.1021/acssensors.9b00994

[39] Xu J, Chen Q, Swain GM (1998) Anthraquinonedisulfonate electrochemistry: a comparison of glassy carbon, hydrogenated glassy carbon, highly oriented pyrolytic graphite, and diamond electrodes. Anal Chem 70:3146. https://doi.org/10.1021/ac9800661

[40] Chang AY, Dutta G, Siddiqui S, Arumugam PU (2019) Surface fouling of ultrananocrystalline diamond microelectrodes during dopamine detection: improving lifetime via electrochemical cycling. ACS Chem Neurosci 10:313. https://doi.org/10.1021/acschemneuro.8b00257

[41] Mei R, Wei Q, Zhu C et al (2019) 3D macroporous boron-doped diamond electrode with interconnected liquid flow channels: a high-efficiency electrochemical degradation of RB-19 dye wastewater under low current. Appl Catal B 245:420

[42] Zeng J, Jean DI, Ji C, Zou S (2012) In situ surface-enhanced Raman spectroscopic studies of nafion adsorption on Au and Pt electrodes. Langmuir 28:957. https://doi.org/10.1021/la2035455

[43] Bernard M, Deneuville A, Muret P (2004) Non-destructive determination of the boron concentration of heavily doped metallic diamond thin films from Raman spectroscopy. Diam Relat Mater 13:282. https://doi.org/10.1016/j.diamond.2003.10.051

[44] Ramamurti R, Becker M, Schuelke T et al (2008) Boron doped diamond deposited by microwave plasma-assisted CVD at low and high pressures. Diam Relat Mater 17:481. https://doi.org/10.1016/j.diamond.2007.08.042

[45] Chai Z, Wang C, Zhang H et al (2010) Nafion-carbon nanocomposite membranes prepared using hydrothermal carbonization for proton-exchange-membrane fuel cells. Adv Func Mater 20:4394. https://doi.org/10.1002/adfm.201001412

[46] Dinesh B, Saraswathi R, Senthil Kumar A (2017) Water based homogenous carbon ink modified electrode as an efficient sensor system for simultaneous detection of ascorbic acid, dopamine and uric acid. Electrochim Acta 233:92. https://doi.org/10.1016/j.electacta.2017.02.139

[47] Nicholson RS, Shain I (1964) Theory of stationary electrode polarography. Single scan and cyclic methods applied to reversible, irreversible, and kinetic systems. Anal Chem 36:706. https://doi.org/10.1021/ac60210a007

[48] Lavagnini I, Antiochia R, Magno F (2004) An extended method for the practical evaluation of the standard rate constant from cyclic voltammetric data. Electroanalysis 16:505. https://doi.org/10.1002/elan.200302851

[49] RJ Klingler, JK Kochi (1980) ChemInform abstract: heterogeneous rates of electron transfer. application of cyclic voltammetric techniques to irreversible electrochemical processes. Chemischer Informationsdienst https://doi.org/10.1002/chin.198040095

[50] Randviir EP (2018) A cross examination of electron transfer rate constants for carbon screen-printed electrodes using electrochemical impedance spectroscopy and cyclic voltammetry. Electrochim Acta 286:179. https://doi.org/10.1016/j.electacta.2018.08.021

[51] Thakur B, Bernalte E, Smith J, et al (2016) The mediatorless electroanalytical sensing of sulfide utilizing unmodified graphitic electrode. Mater C https://doi.org/10.3390/c2020014

[52] Jiang L, Nelson GW, Abda J, Foord JS (2016) Novel modifications to carbon-based electrodes to improve the electrochemical detection of dopamine. ACS Appl Mater Interfaces 8:28338. https://doi.org/10.1021/acsami.6b03879

[53] Pruneanu S, Biris AR, Pogacean F et al (2015) The influence of uric and ascorbic acid on the electrochemical detection of dopamine using graphene-modified electrodes. Electrochim Acta 154:197. https://doi.org/10.1016/j.electacta.2014.12.046

[54] Plowman BJ, Mahajan M, O'Mullane AP, Bhargava SK (2010) Electrochemical detection of dopamine and cytochrome c at a nanostructured gold electrode. Electrochim Acta 55:8953. https://doi.org/10.1016/j.electacta.2010.08.045

[55] Currie LA (1999) Nomenclature in evaluation of analytical methods including detection and quantification capabilities. Anal Chim Acta 391:105. https://doi.org/10.1016/S0003-2670(99)00104-X

[56] Reymond MJ, Speciale SG, Porter JCJE (1983) Dopamine in plasma of lateral and medial hypophysial portal vessels: evidence for regional variation in the release of hypothalamic dopamine into hypophysial portal blood. Endocrinology 112:1958

[57] Sun CL, Lee HH, Yang JM, Wu CC (2011) The simultaneous electrochemical detection of ascorbic acid, dopamine, and uric acid using graphene/size-selected Pt nanocomposites. Biosens Bioelectron 26:3450. https://doi.org/10.1016/j.bios.2011.01.023

[58] Ping J, Wu J, Wang Y, Ying Y (2012) Simultaneous determination of ascorbic acid, dopamine and uric acid using high-performance screen-printed graphene electrode. Biosens Bioelectron 34:70. https://doi.org/10.1016/j.bios.2012.01.016

[59] Manivel P, Dhakshnamoorthy M, Balamurugan A, Ponpandian N, Mangalaraj D, Viswanathan C (2013) Conducting polyaniline-graphene oxide fibrous nanocomposites: preparation, characterization and simultaneous electrochemical detection of ascorbic acid, dopamine and uric acid. RSC Adv. https://doi.org/10.1039/c3ra42322k

[60] Jiang J, Du X (2014) Sensitive electrochemical sensors for simultaneous determination of ascorbic acid, dopamine, and uric acid based on Au@Pd-reduced graphene oxide nanocomposites. Nanoscale 6:11303. https://doi.org/10.1039/c4nr01774a

[61] Zhang X, Zhang Y-C, Ma L-X (2016) One-pot facile fabrication of graphene-zinc oxide composite and its enhanced sensitivity for simultaneous electrochemical detection of ascorbic acid, dopamine and uric acid. Sensors Actuat B: Chem 227:488. https://doi.org/10.1016/j.snb.2015.12.073

[62] Bao Y, Song J, Mao Y et al (2011) Graphene oxide-templated polyaniline microsheets toward simultaneous electrochemical determination of AA/DA/UA. Electroanalysis 23:878. https://doi.org/10.1002/elan.201000607

[63] Sheng ZH, Zheng XQ, Xu JY, Bao WJ, Wang FB, Xia XH (2012) Electrochemical sensor based on nitrogen doped graphene: simultaneous determination of ascorbic acid, dopamine and uric acid. Biosens Bioelectron 34:125. https://doi.org/10.1016/j.bios.2012.01.030

[64] Noroozifar M, Khorasani-Motlagh M, Akbari R, Bemanadi Parizi M (2011) Simultaneous and sensitive determination of a quaternary mixture of AA, DA, UA and Trp using a modified GCE by iron ion-doped natrolite zeolite-multiwall carbon nanotube. Biosens Bioelectron 28:56. https://doi.org/10.1016/j.bios.2011.06.042

[65] Cui R, Wang X, Zhang G, Wang C (2012) Simultaneous determination of dopamine, ascorbic acid, and uric acid using helical carbon nanotubes modified electrode. Sensors Actuat B Chem 161:1139. https://doi.org/10.1016/j.snb.2011.11.040

[66] Ensafi AA, Taei M, Khayamian T, Arabzadeh A (2010) Highly selective determination of ascorbic acid, dopamine, and uric acid by differential pulse voltammetry using poly(sulfonazo III) modified glassy carbon electrode.

Sensors and Actuators B: Chemical 147:213. https://doi.org/10.1016/j.snb.2010.02.048

[67] Tian X, Cheng C, Yuan H et al (2012) Simultaneous determination of L-ascorbic acid, dopamine and uric acid with gold nanoparticles-beta-cyclodextrin-graphene-modified electrode by square wave voltammetry. Talanta 93:79. https://doi.org/10.1016/j.talanta.2012.01.047

[68] Hathoot AA, Hassan KM, Essa WA, Abdel-Azzem M (2017) Simultaneous determination of ascorbic acid, uric acid and dopamine at modified electrode based on hybrid nickel hexacyanoferrate/poly(1,5-diaminonaphthalene). J Iran Chem Soc 14:1789. https://doi.org/10.1007/s13738-017-1119-8

[69] Aydoğdu Tığ G, Günendi G, Pekyardımcı Ş (2017) A selective sensor based on Au nanoparticles-graphene oxide-poly(2,6-pyridinedicarboxylic acid) composite for simultaneous electrochemical determination of ascorbic acid, dopamine, and uric acid. J Appl Electrochem 47:607. https://doi.org/10.1007/s10800-017-1060-7

[70] Filik H, Avan AA, Aydar S (2016) Simultaneous detection of ascorbic acid, dopamine, uric acid and tryptophan with Azure A-interlinked multi-walled carbon nanotube/gold nanoparticles composite modified electrode. Arab J Chem 9:471. https://doi.org/10.1016/j.arabjc.2015.01.014

[71] Vicentini FC, Raymundo-Pereira PA, Janegitz BC, Machado SAS, Fatibello-Filho O (2016) Nanostructured carbon black for simultaneous sensing in biological fluids. Sensors Actuat B Chem 227:610. https://doi.org/10.1016/j.snb.2015.12.094

[72] Yang C, Wang Y, Jacobs CB, Ivanov IN, Venton BJ (2017) O2 Plasma Etching and Antistatic Gun Surface Modifications for CNT Yarn Microelectrode Improve Sensitivity and Antifouling Properties. Anal Chem 89:5605. https://doi.org/10.1021/acs.analchem.7b00785

[73] Ruslinda AR, Ishiyama Y, Penmatsa V, Ibori S, Kawarada H (2015) Repulsive effects of hydrophobic diamond thin films on biomolecule detection. Appl Surface Sci 328:314. https://doi.org/10.1016/j.apsusc.2014.12.011

[74] Escobar JV, Garza C, Alonso JC, Castillo R (2013) Supermercuryphobic and hydrophobic diamond surfaces with hierarchical structures: vanishment of the contact angle hysteresis with mercury. Appl Surface Sci 273:692. https://doi.org/10.1016/j.apsusc.2013.02.114